

NASA/TM—2008-215147



Strength, Fatigue, and Fracture Toughness of Ti-6Al-4V Liner From a Composite Over- Wrapped Pressure Vessel

*Jonathan A. Salem, Brad Lerch, John C. Thesken, and Jim Sutter
Glenn Research Center, Cleveland, Ohio*

*Richard Russell
Kennedy Space Center, Kennedy Space Center, Florida*

NASA STI Program . . . in Profile

Since its founding, NASA has been dedicated to the advancement of aeronautics and space science. The NASA Scientific and Technical Information (STI) program plays a key part in helping NASA maintain this important role.

The NASA STI Program operates under the auspices of the Agency Chief Information Officer. It collects, organizes, provides for archiving, and disseminates NASA's STI. The NASA STI program provides access to the NASA Aeronautics and Space Database and its public interface, the NASA Technical Reports Server, thus providing one of the largest collections of aeronautical and space science STI in the world. Results are published in both non-NASA channels and by NASA in the NASA STI Report Series, which includes the following report types:

- **TECHNICAL PUBLICATION.** Reports of completed research or a major significant phase of research that present the results of NASA programs and include extensive data or theoretical analysis. Includes compilations of significant scientific and technical data and information deemed to be of continuing reference value. NASA counterpart of peer-reviewed formal professional papers but has less stringent limitations on manuscript length and extent of graphic presentations.
- **TECHNICAL MEMORANDUM.** Scientific and technical findings that are preliminary or of specialized interest, e.g., quick release reports, working papers, and bibliographies that contain minimal annotation. Does not contain extensive analysis.
- **CONTRACTOR REPORT.** Scientific and technical findings by NASA-sponsored contractors and grantees.
- **CONFERENCE PUBLICATION.** Collected

papers from scientific and technical conferences, symposia, seminars, or other meetings sponsored or cosponsored by NASA.

- **SPECIAL PUBLICATION.** Scientific, technical, or historical information from NASA programs, projects, and missions, often concerned with subjects having substantial public interest.
- **TECHNICAL TRANSLATION.** English-language translations of foreign scientific and technical material pertinent to NASA's mission.

Specialized services also include creating custom thesauri, building customized databases, organizing and publishing research results.

For more information about the NASA STI program, see the following:

- Access the NASA STI program home page at <http://www.sti.nasa.gov>
- E-mail your question via the Internet to help@sti.nasa.gov
- Fax your question to the NASA STI Help Desk at 301-621-0134
- Telephone the NASA STI Help Desk at 301-621-0390
- Write to:
NASA Center for AeroSpace Information (CASI)
7115 Standard Drive
Hanover, MD 21076-1320



Strength, Fatigue, and Fracture Toughness of Ti-6Al-4V Liner From a Composite Over- Wrapped Pressure Vessel

*Jonathan A. Salem, Brad Lerch, John C. Thesken, and Jim Sutter
Glenn Research Center, Cleveland, Ohio*

*Richard Russell
Kennedy Space Center, Kennedy Space Center, Florida*

Prepared for the
Aging Aircraft 2008
sponsored by the NASA, FAA, U.S. Department of Defense, and ICAA
Phoenix, Arizona, April 21–24, 2008

National Aeronautics and
Space Administration

Glenn Research Center
Cleveland, Ohio 44135

Acknowledgments

The authors thank Chris Burke for mechanical testing, Joy Buehler for metallography, Terry McCue for microprobe analysis, Rick Rogers for X-ray, Mark Jaster for heat treatments, Derek Johnson for chemistry, Ralph Corner for dynamic modulus, Tony Kapucinski for specimen machining, and Ramesh Kalluri for useful discussions.

This report is a preprint of a paper intended for presentation at a conference. Because changes may be made before formal publication, this preprint is made available with the understanding that it will not be cited or reproduced without the permission of the author.

Level of Review: This material has been technically reviewed by technical management.

Available from

NASA Center for Aerospace Information
7115 Standard Drive
Hanover, MD 21076-1320

National Technical Information Service
5285 Port Royal Road
Springfield, VA 22161

Available electronically at <http://gltrs.grc.nasa.gov>

Strength, Fatigue, and Fracture Toughness of Ti-6Al-4V Liner From a Composite Over-Wrapped Pressure Vessel

Jonathan A. Salem, Brad Lerch, John C. Thesken, and Jim Sutter
National Aeronautics and Space Administration
Glenn Research Center
Cleveland, Ohio 44135

Richard Russell
National Aeronautics and Space Administration
Kennedy Space Center
Kennedy Space Center, Florida 32899

Summary

It was demonstrated by way of experiment that Composite Over-wrapped Pressure Vessel (COPV) Ti-6Al-4V liner material can sustain the expected service loads and cycles. The experiments were performed as part of investigations on the residual life of COPV tanks being used in Space Shuttle Orbiters. Measured properties included tensile strength, compressive strength, reversed loading cycles to simulate liner proof strains, and cyclic fatigue loading to demonstrate the ability to sustain 1000 cycles after liner buckling. The liner material came from a salvaged 40 in. Columbia (orbiter 102) tank (SN029), and tensile strength measurements were made on both boss-transition (thick) and membrane regions (thin).

The average measured yield strength was 131 ksi in the boss-transition and membrane regions, in good agreement with measurements made on 1970's vintage forged plate stock. However, Young's modulus was 17.4 ± 0.3 Msi, somewhat higher than typical handbook values (~16 Msi). The fracture toughness, as estimated from a failed fatigue specimen, was $74 \text{ ksi}\sqrt{\text{in}}$, in reasonable agreement with standardized measurements made on 1970's vintage forged plate stock. Low cycle fatigue of a buckled test specimen implied that as-imprinted liners can sustain over 4000 load cycles.

Introduction

Composite Over-Wrapped Pressure Vessels (COPV) are used to supply helium and nitrogen to space shuttle systems such as the Reaction Control System (RCS), Environmental Control and Life Support System (ECLSS), Main Propulsion System (MPS), and the Orbital Maneuvering System (OMS). The gases are stored under high pressure and thus catastrophic failure must be avoided. To save weight and enhance reliability, the vessels consist of a titanium liner that is over-wrapped with Kevlar fibers. Over time, the titanium liner may degrade by cyclic fatigue and the Kevlar overwrap may degrade by creep relaxation and environmental decay.

The COPV's in Endeavor (orbiter 105), Atlantis (orbiter 104), and Discovery (orbiter 103) have exceeded the original design certification (10 years) and thus much investigation into the reliability of these COPV's has been conducted. This paper summarizes mechanical testing, metallography and chemical analysis of the titanium-6 percent aluminum-4 percent vanadium (Ti-6Al-4V) liner in COPV SN029 (designated as debris article 2152) which supported operation of Space Shuttle Columbia.

Experimental Procedures

Test Specimen Extraction

The Columbia 40 in. Orbital Maneuvering System tank SN029 was sectioned into hemispheres along the polar axis and the composite over wrap removed to expose the Ti-6Al-4V liner. Three plaques from the relatively thick boss-transition region were excised and machined into flat, 4 in. long sub-sized ASTM E08 (ref. 1) tensile specimens by electro-discharge machining (EDM) and surface milling. Both equatorial and polar orientations were removed, as shown in figure 1. Because of the relative thickness of the boss region, the specimens are believed to represent mill annealed Ti-6Al-4V without cold work despite the autofrettage cycle.

In addition, four plaques were removed from the membrane region and sectioned into a total of 40 polar and equatorial tensile specimens with the original tank surfaces and curvature. Because of the thinness of the membrane region, the specimens are believed to represent mill annealed Ti-6Al-4V subjected to cold work (1.2 percent biaxial strain) via the autofrettage cycle.

Chemistry and Metallography

Remnant pieces from cutting the gage section into tensile blanks were used for chemical analysis and to produce metallographic views in polar, equatorial and surface (radial) directions relative to the liner axes. The specimens were polished by using a solution of 300 ml colloidal silica (60/40 solution with H₂O), 30 ml H₂O₂ and 30 ml NH₄OH, and etched by using Kroll's reagent (2 ml HF, 8 ml HNO₃, 90 ml H₂O for 3 to 5 sec).

During tank sectioning, a distinct blue oxide layer with dark brown spots was observed on the inside of the tank. The dark spots were speculated to result from either weld splatter or corrosion. The source of the blue oxidation, as reported in the data pack for COPV SN022, was poor atmospheric control during solution treatment and aging of the liner after welding. The data pack indicated that no alpha case¹ was present, and that witness coupons exhibited acceptable tensile properties. The data pack also indicated that the blue layer was removed from the tank exterior by polishing with an abrasive pad (i.e., Scotchbrite) followed by dipping in acid.

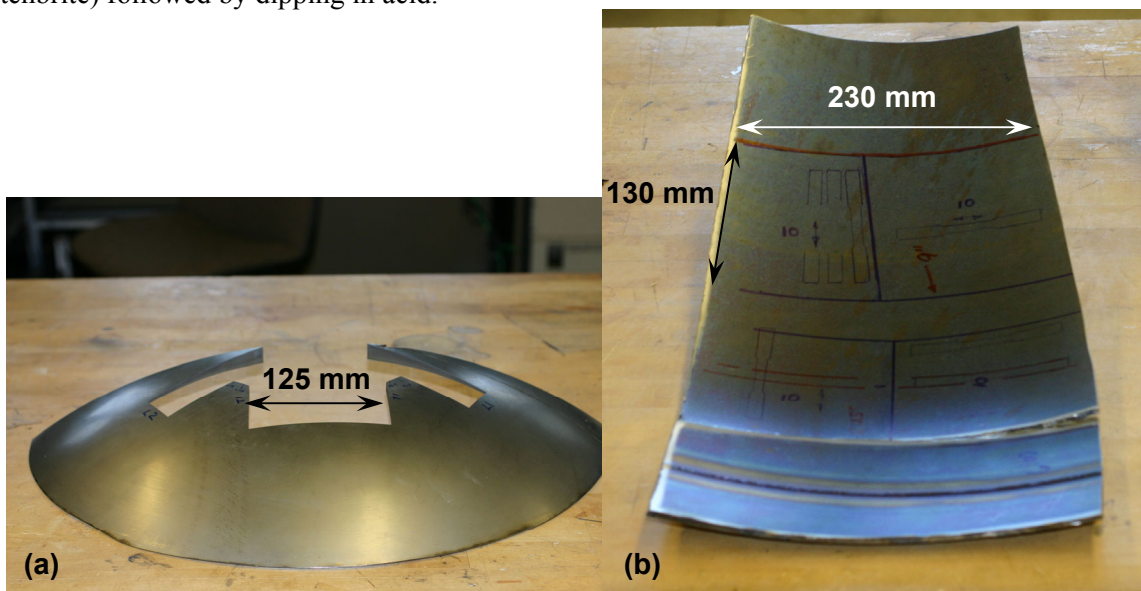


Figure 1.—Removal pattern for tensile specimens: (a) boss-transition region and (b) membrane region.

¹Alpha case is the oxygen, nitrogen or carbon enriched, alpha stabilized, brittle surface which results from elevated temperature exposure.

The depth and chemistry of the spots were investigated via metallography and etching with a solution of 2 ml HF and 98 ml H₂O. Polished cross sections of the oxide layer with a nickel protective coating were analyzed by EDS (energy dispersive spectroscopy) and x-ray mapping.

Tensile Testing

Tensile specimens were tested in stroke control at 0.025 in. per minute with a fixed grip system. Upon yield, the stroke rate was increased to 0.060 in. per minute. This typically resulted in a stress rate of 125 ksi per minute. The curvature of the membrane region specimens was ignored and the specimens straightened somewhat by clamping in the grips. Strains were determined with an extensometer and strain gages. Yield strength was determined by the 0.2 percent offset method described in ASTM E08 (ref. 1). Young's modulus in tension and compression was determined by linear regression of stress-strain data over a variety of regions because the liners are subjected to a range of loads from post-yield tension during autofrettage to compression at zero pressure.

In addition, Young's modulus in compression was determined by loading three boss-transition specimens as described previously to ~50 percent of the yield strength in tension followed by 50 percent in compression.

Besides measuring the static modulus of the material, the dynamic modulus and Poisson's ratio were determined between room temperature and 1650 °F by using impulse excitation per ASTM E1876 (ref. 2).

Cyclic Loading

Autofrettage simulation

The behavior of the titanium liner during autofrettage influences the residual stress in both the Kevlar overwrap and liner, and thereby influences vessel life. In order to better understand the residual stress levels in the Kevlar over wrap and the observed behavior of another COPV, SN011, during burst testing, tensile specimens were loaded to simulate proof cycles and the burst cycle. Because the vessels are subjected to biaxial stresses, equivalent stresses for uniaxial testing were estimated by assuming isotropy and using von Mises criterion, constancy of volume, Hook's law and effective Poisson's ratio based on the fraction of plasticity:

$$\epsilon_{eq} = \frac{1}{(1 + \nu_{eff})\sqrt{2}} \sqrt{(\epsilon_1 - \epsilon_2)^2 + (\epsilon_2 - \epsilon_3)^2 + (\epsilon_3 - \epsilon_1)^2} \quad (1)$$

$$V_i = V_f \quad (2)$$

$$\epsilon_3 = \left(\frac{-\nu_{eff}}{1 - \nu_{eff}} \right) (\epsilon_1 + \epsilon_2) \quad (3)$$

$$\nu_{eff} = \nu_e \left(\frac{\epsilon_e}{\epsilon_T} \right) + \nu_p \left(\frac{\epsilon_p}{\epsilon_T} \right) \quad (4)$$

where the equivalent, elastic, plastic, principal direction ($i = 1,2,3$), and total strains are given by ϵ_{eq} , ϵ_e , ϵ_p , ϵ_i , and ϵ_T respectively, and ν_e , ν_p , and ν_{eff} are the elastic, plastic and effective values of Poisson's ratio. V_i and V_f are the initial and final volumes of an element of material.

During the testing it was noted that the Ti-6Al-4V exhibited a Bauschinger effect, and several additional load cycles were performed to investigate the effect.

Fatigue loading

During boroscope inspections of several vessels at White Sands Test Facility (WSTF), the ripple patterns shown in figure 2 were observed. This pattern was attributed to either buckling of the liner during proof cycling or imprinting of the over-wrap pattern on the liner. In either event, the resultant ripples imply larger than ideal surface strains and thus some simulation of the fatigue life was deemed necessary. Similar but smaller patterns were noted on SN029 during inspections at NASA Glenn Research Center.

Measurements of the imprints on SN029 via the dial gage in figure 3 indicated a maximum displacement of ± 0.002 in. from the nominal centerline over a typical spacing of 1.25 in.

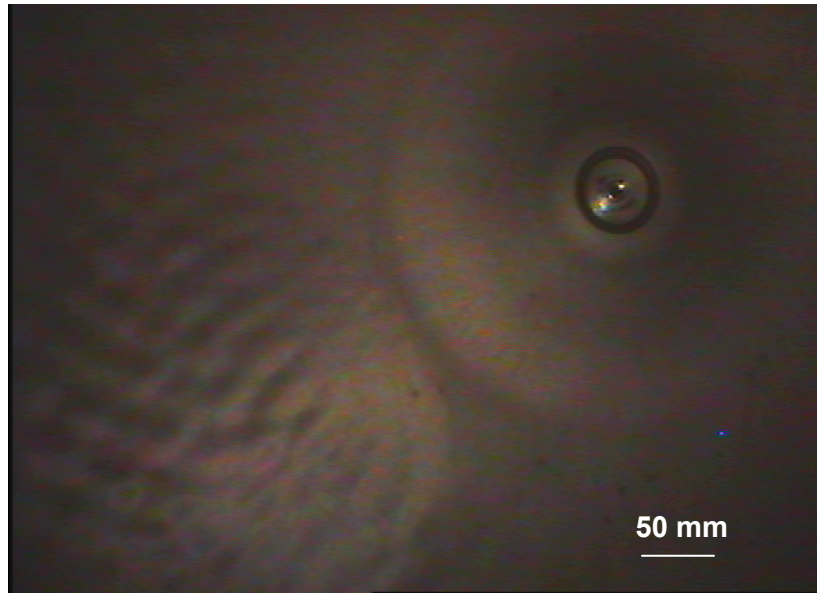


Figure 2.—Ripple patterns or imprints observed inside tank SN022.

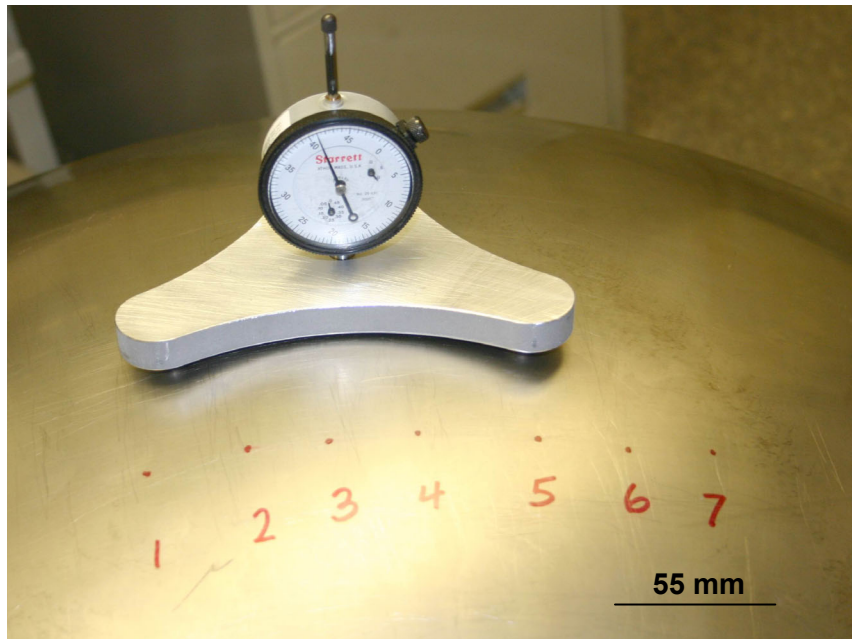


Figure 3.—Dial gage setup used to measure ripples in SN029. The points labeled 1 to 7 locate elliptical ripples or imprints on the tank liner.

To simulate liner loading, a tensile specimen that had been loaded to the proof strain and buckled was subjected to fatigue loading between a tensile strain corresponding to the Maximum Expected Operating Pressure (MEOP) and the compression strain corresponding to a total biaxial strain range of 0.7 percent. The test was performed in load control to avoid extensometer slippage, loss of system control, and contaminant damage of the test specimen. Extensometer slippage occurred only once, on the 49th cycle. The initial loading was estimated from autofrettage simulation cycles and had to be adjusted to obtain the desired strain. The actual loading was between approximately 100 and –60 ksi for the first 2,134 cycles and between 105 and –75 ksi for the balance of specimen life.

Results

Chemistry and Metallography

Table 1 gives chemical analysis results for the boss-transition region. The chemistry meets MIL-T-9047G requirements. Metallographic views of the boss-transition region are shown in figure 4. Planes normal to the polar and equatorial axes exhibit similar structure, however, the liner surface plane exhibits a coarser structure that does not correlate with either polar or equatorial views implying some variation in grain size through the thickness. This difference in grain size was also noted during x-ray diffraction measurements: diffraction patterns from the shell surface exhibit discontinuous Debye rings whereas patterns from the depth exhibited continuous lines, implying a grain structure difference. Views of the membrane region, which are more consistent, are shown in figure 5. Additional metallography of the boss transition region did not reveal a consistent through-thickness difference in structure. The microstructures in figures 4 and 5 are typical of those exhibited by Ti-6V-4Al.

TABLE 1.—CHEMICAL ANALYSIS OF THE BOSS-TRANSITION REGION OF SN029 IN WEIGHT PERCENT

Ti	Al	C	Fe	N	O	S	Si	V
88.97	6.24	0.0089	0.25	0.0092	0.163	0.0056	0.015	4.15

Observation of the cross section of the spots shown in figure 6 did not indicate significant depth or microstructural anomalies. The oxide layer was very thin ($< 1 \mu\text{m}$) and no alpha case was apparent. Of more interest was the small, transgranular cracks emanating from the interior surface into alpha grains in the membrane region, as shown in figures 7 and 8. The cracks were speculated to be due to increased oxygen content.

Further inspection using scanning electron microscopy indicated a network of transgranular cracks on the oxidized surface, as shown in figure 9. No cracks were apparent on the exterior surface (fig. 10), however, as discussed previously, the SN022 data pack indicates that the oxide layer was removed by polishing with an abrasive pad followed by an acid dip.

The average depth (into the tank surface) of 21 cracks emanating from the interior edge of metallographic planes normal to the equatorial direction of the membrane region was $10 \pm 4 \mu\text{m}$. Observation of 28 cracks on planes normal to the polar direction indicated a significantly smaller average crack size of $5 \pm 3 \mu\text{m}$. A maximum crack length of $20 \mu\text{m}$ was observed. Much smaller, much less frequent cracks could be observed emanating from the tank exterior, implying that the polishing and etching process (described in the SN022 data pack) reduced the crack size. The bulk of the most visible cracks appeared to be nearly normal to the equatorial direction, however, cracks could be observed at other angles and determination of any bias in the crack pattern would require more significant sampling.

In contrast to the membrane region, metallographic sections of the boss-transition region revealed no surface cracking, likely a result of the lower stresses during autofrettage and service. Because of concerns that stresses and thus cracking around the dimples/impressions are higher, an imprint was sectioned and measurements of the cracks were performed. The average crack depth from 30 observations along the interior edge of metallographic planes normal to the equatorial direction was $7 \pm 4 \mu\text{m}$. Observation of 30 cracks on planes normal to the polar direction indicated a similar crack depth of $7 \pm 5 \mu\text{m}$. A maximum crack depth of $18 \mu\text{m}$ was observed.

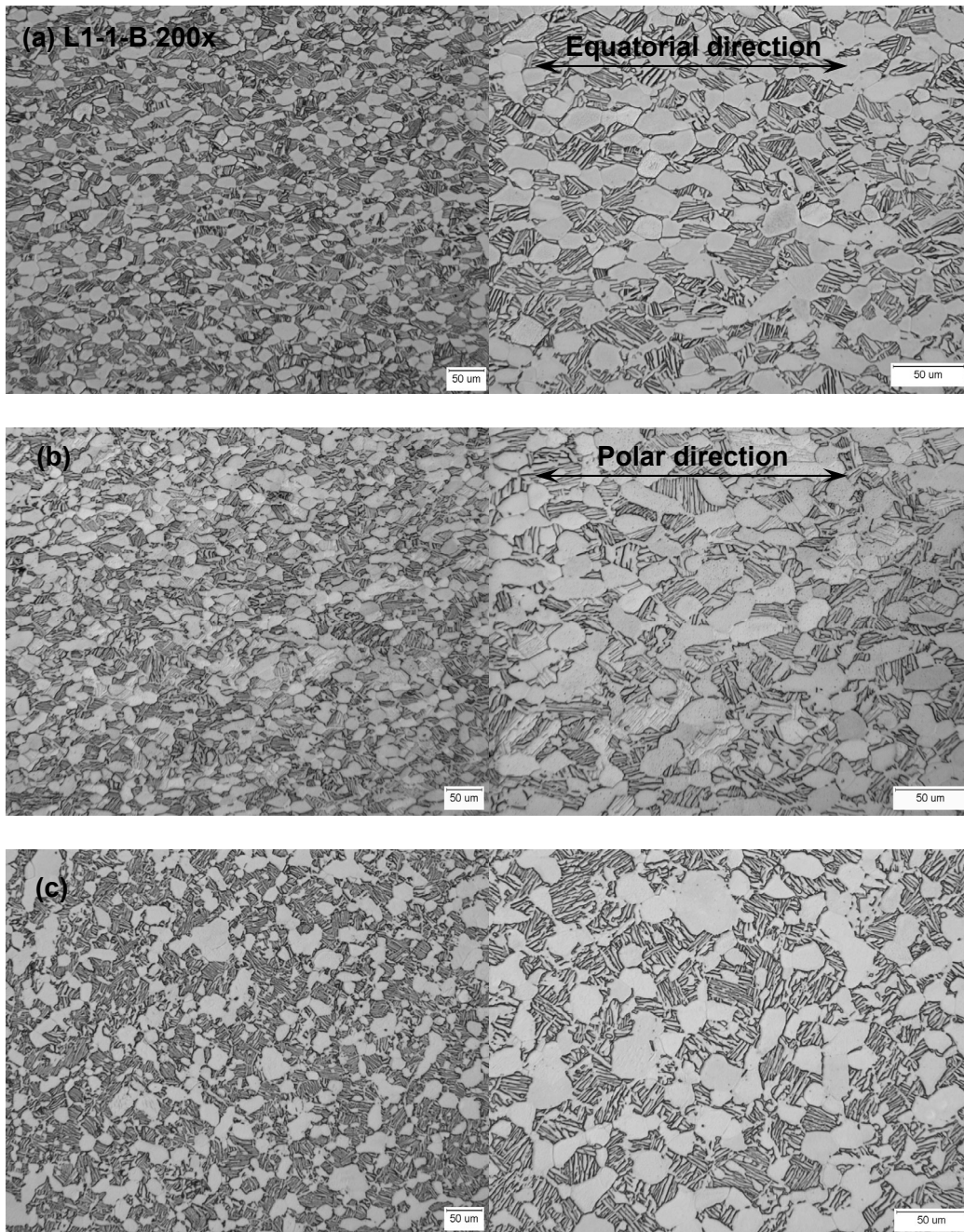


Figure 4.—Metallographic views from the boss-transition region at two magnifications: (a) in the equatorial direction, (b) in the polar direction, and (c) into the vessel surface (radial).

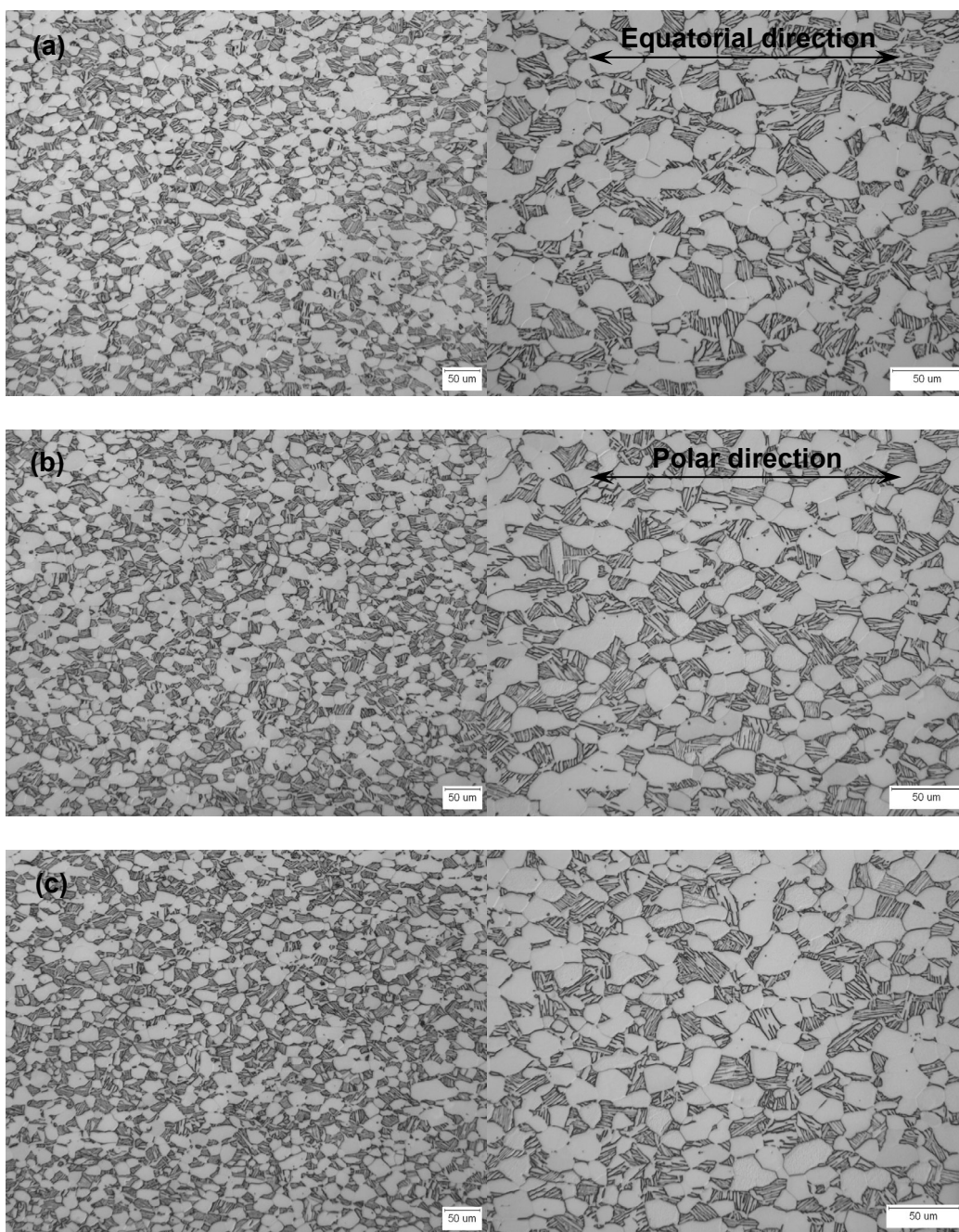


Figure 5.—Metallographic views from the membrane region at two magnifications: (a) in the equatorial direction, (b) in the polar direction, and (c) into the vessel surface (radial).

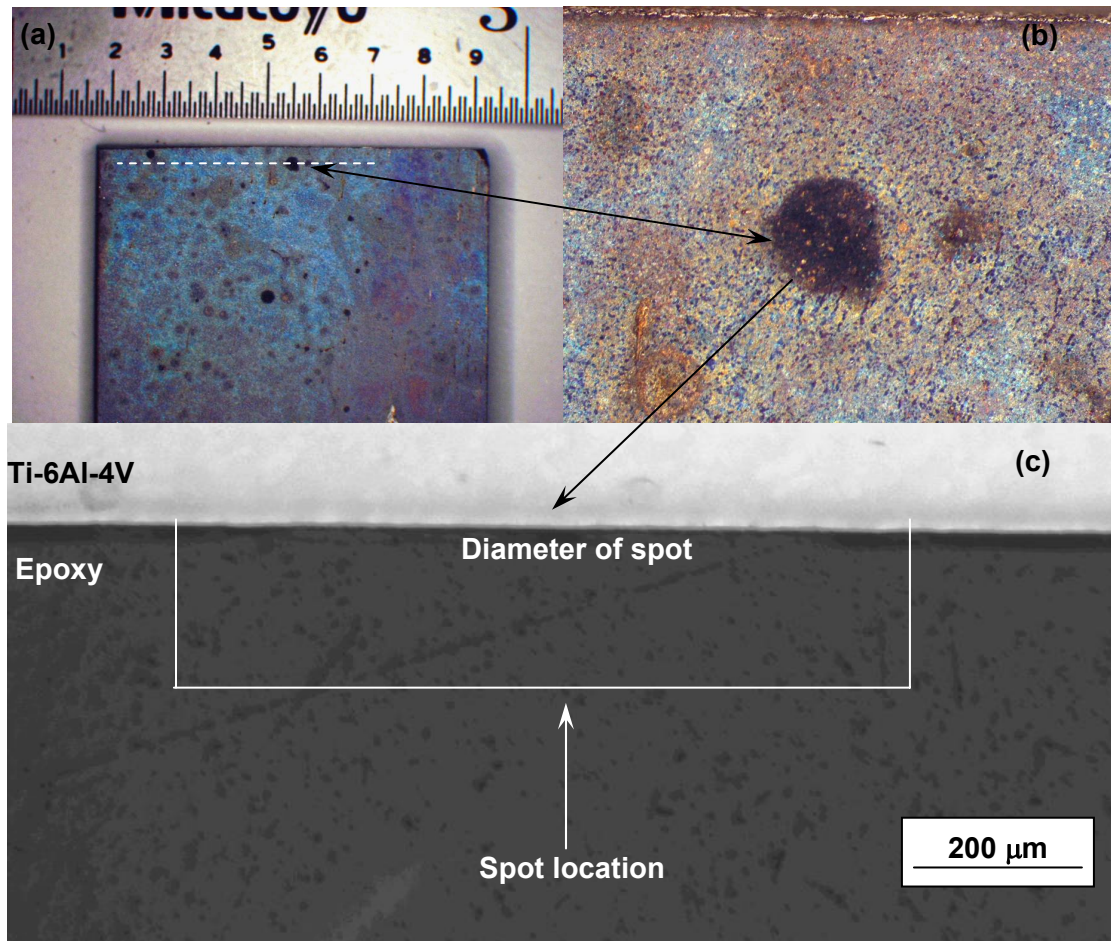


Figure 6.—(a) and (b) Interior surface of liner showing blue heat tint and presence of spots. Dashed line indicates location of metallographic views. (c) Cross section of the spot.

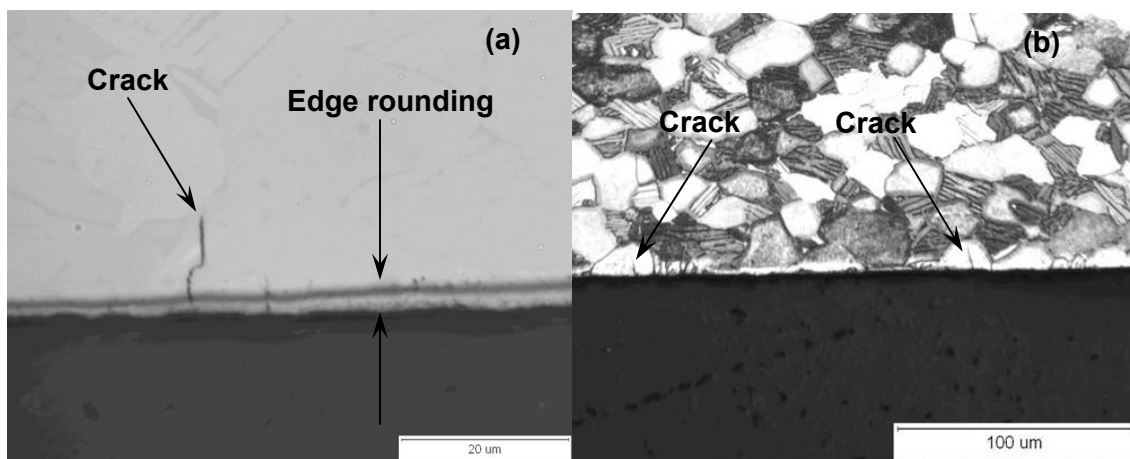


Figure 7.—Small surface cracks emanating from the tank interior at the spot: (a) as-polished and (b) etched.

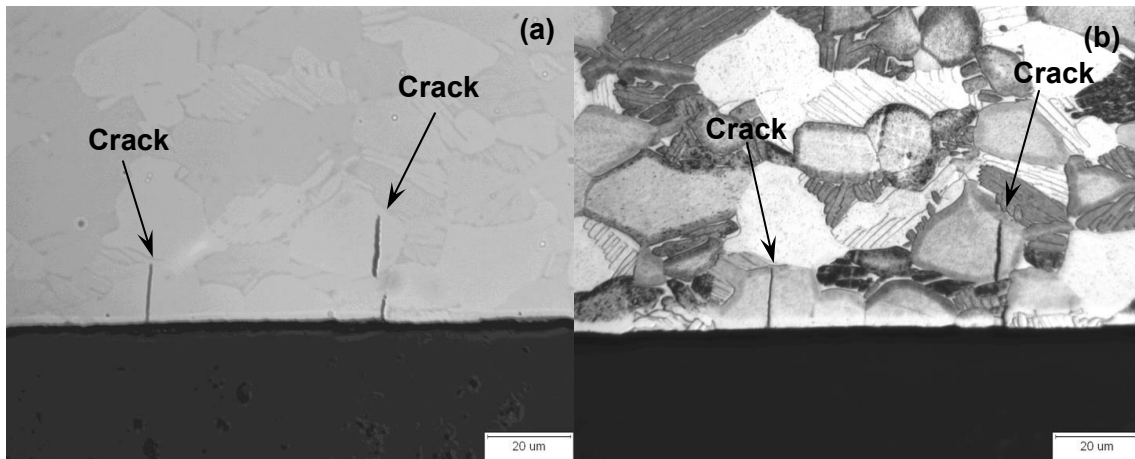


Figure 8.—Small surface cracks emanating from the tank interior away from the spot: (a) as-polished and (b) etched.

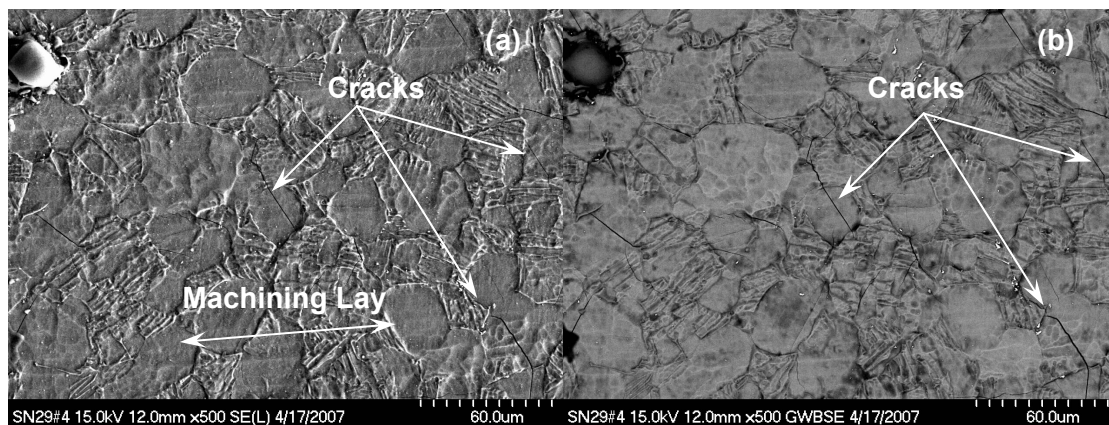


Figure 9.—Cracks on the inner surface of the liner as viewed with (a) secondary and (b) back scattered electrons.

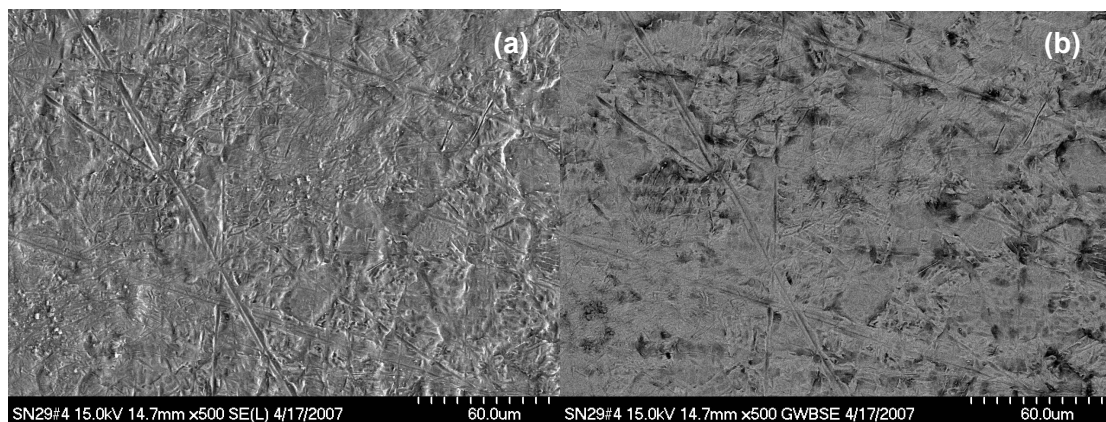


Figure 10.—Exterior surface of the liner as viewed with (a) secondary and (b) back scattered electrons. Cracks are not visible.

Chemical analysis of the spots via EDS indicated carbon, as shown in figure 11, implying that the spots are carbonaceous stains rather than corrosion. Chemical analysis of the oxygen content near the interior surface via EDS and microprobe x-ray mapping did not indicate increased oxygen or carbon content, as shown in figures 12 and 13. All elemental maps, with the exception of nickel, exhibit a uniform distribution from the interior to the edge, implying insignificant compositional change. Thus chemical variation cannot be used to construe embrittlement.

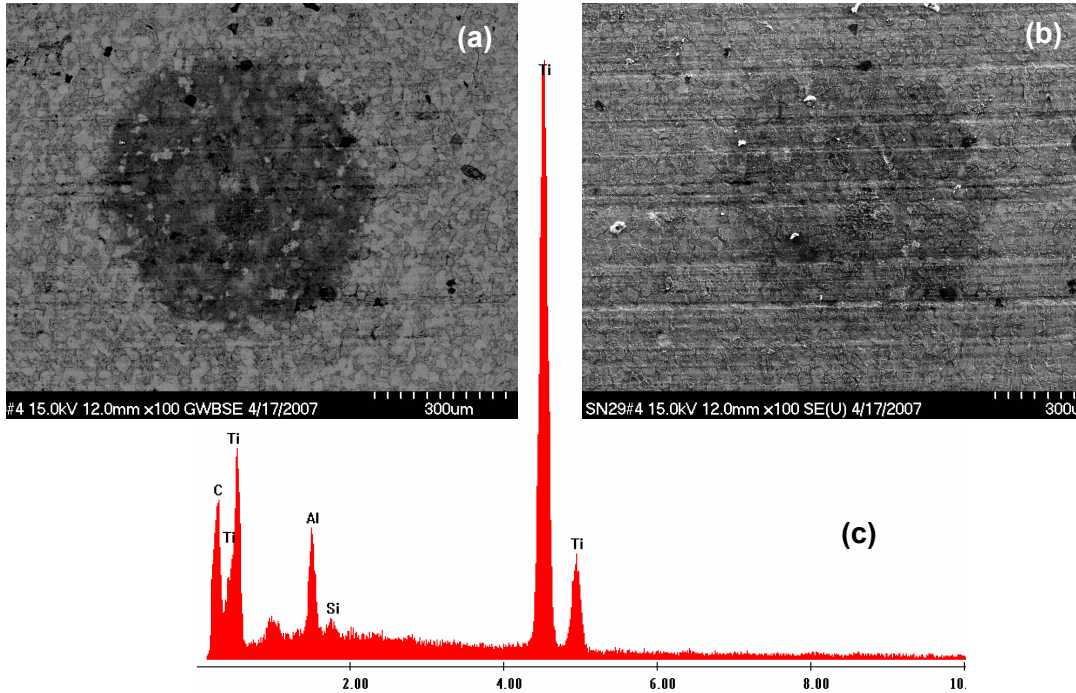


Figure 11.—Spots as viewed with (a) backscattered and (b) secondary electrons. (c) Chemical analysis indicating the presence of carbon.

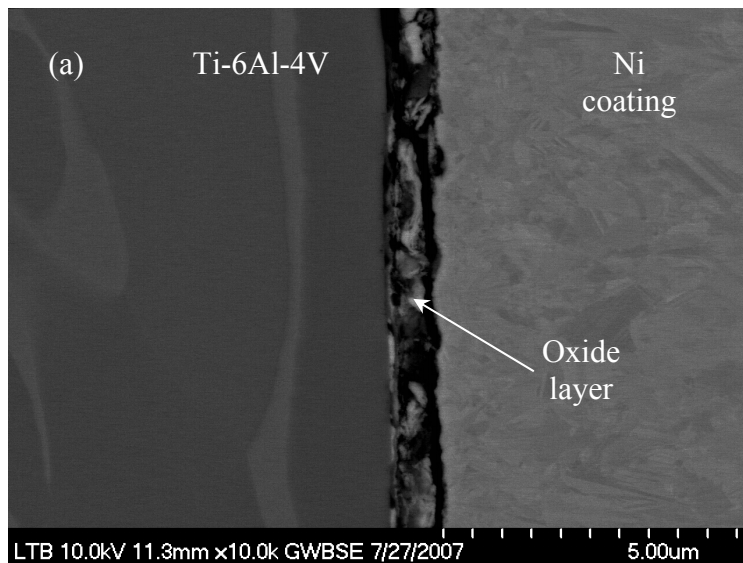


Figure 12.—(a) Cross section of oxide layer.

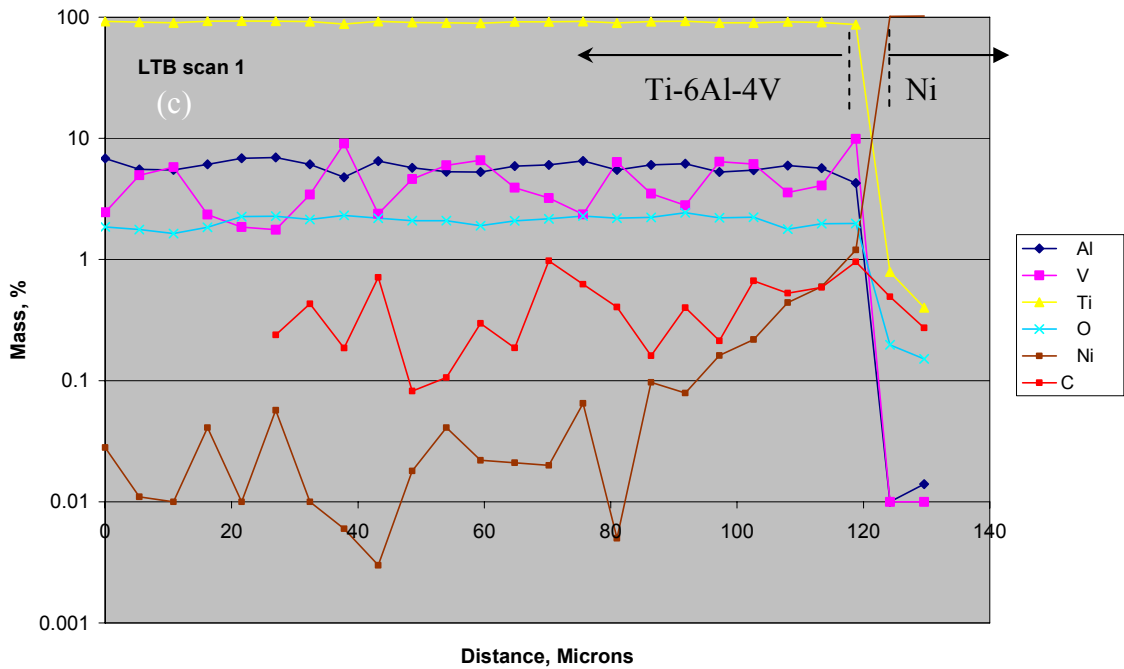
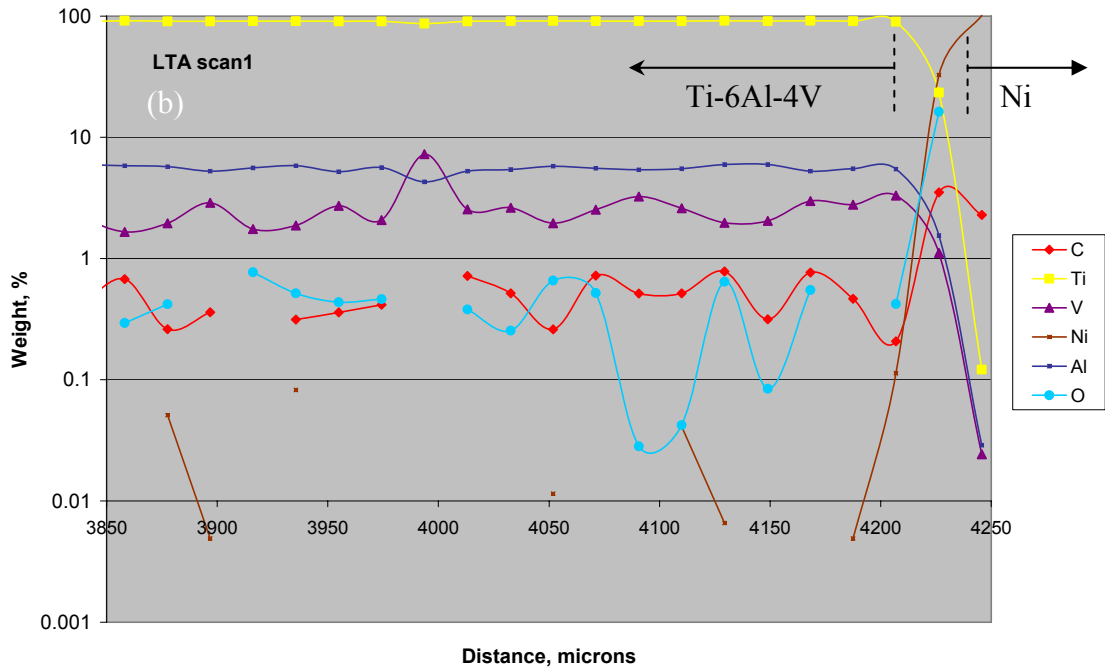


Figure 12.—Concluded. (b), (c) elemental line scans of the near surface region.

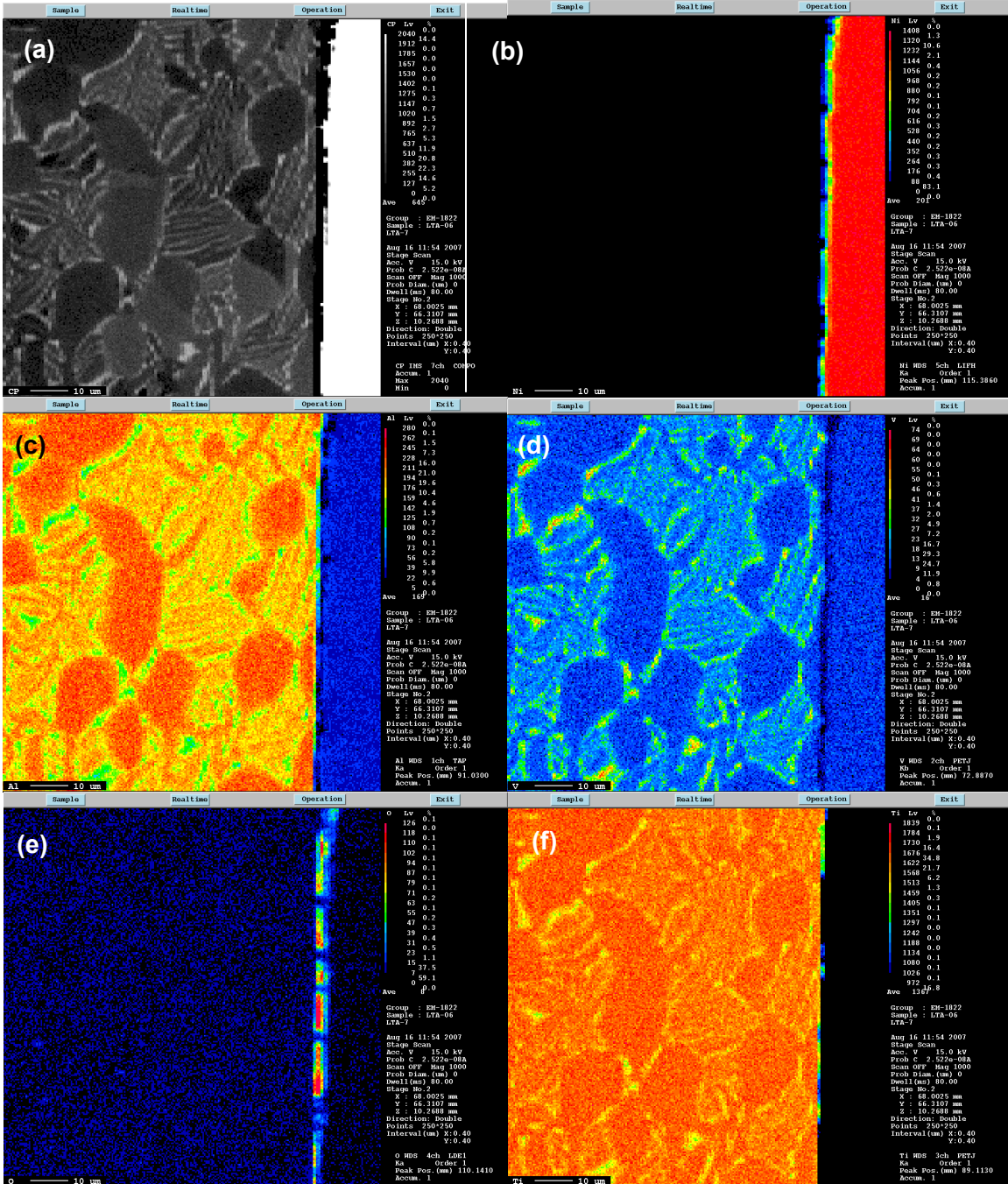


Figure 13.—X-ray composition maps near the oxidized (interior surface) of the vessel: (a) back-scattered electron image, (b) nickel, (c) aluminum, (d) vanadium, (e) oxygen, and (f) titanium. For (a), lighter colors imply higher atomic number elements. For (b) through (f), Reds and yellows imply high concentrations of the specified element, while blues and blacks imply low concentrations.

The gradual change in nickel is due to smearing of the coating during polishing. Thus the hypothesis that the microcracks are due to increased oxygen content, contaminant alpha grain embrittlement and the autofrettage cycle cannot be established. The cause of the cracks is unknown, but they may be due to the brittle oxide layer and the autofrettage cycle.

Tensile Properties

Tensile properties are summarized in tables 2 and 3. The 0.2 percent yield strength, ultimate strength and elongation are comparable to that reported for annealed sheet and bar (ref. 3), and to that measured at NASA Glenn Research Center on 3.5 in. thick alpha-beta forged plate manufactured in 1970 (table 4) (ref. 4), implying that the autofrettage cycle has little effect on the tensile-ductility properties. Annealing of membrane specimens did not change the measured tensile properties. Typical stress-strain curves are shown in figure 14. Strains beyond 10 percent were not recorded due to extensometer range limitations. No strength dependence upon orientation was apparent, and excellent tensile ductility was exhibited relative to Ti-6Al-4V with and without elevated temperature oxygen exposure (ref. 5).

However, Young's modulus in tension and compression, as measured via an extensometer, were slightly higher than that reported (16.0 Msi in tension (ref. 3)). The measured tensile modulus of boss region was 17.5 ± 0.3 Msi, in agreement with measurements of 17.2 ± 0.21 Msi made in the 1980's at GRC on 1970's vintage alpha-beta forged plate. The measured compressive modulus of one boss-transition specimen taken to yield was 17.4 Msi, whereas that previously reported is 16.5 Msi for compression (ref. 3). Also, tensile and compressive moduli of three specimens that were cycled once between approximately ± 50 ksi prior to strength testing were even higher at 17.6 ± 0.4 and 17.8 ± 0.5 Msi, respectively, due to the narrow, low stress used and the dependence upon the range of data used in regression. Membrane specimens exhibit lower elastic modulus, however, the large initial curvature is likely responsible.

TABLE 2.—TENSILE PROPERTIES OF THE BOSS-TRANSITION REGION, 1 INCH GAGE SECTION

SN029 2152	Young's modulus, E Msi	0.2% Yield strength, S_{ys} ksi	Ultimate strength, S_u ksi	Fracture stress, S_f ksi	Elongation e_f %	Area reduction, RA %
Polar axis, (Longitudinal)						
L1-A	17.2	131.2	139.1	119.9	16	33
L1-B	17.4	130.2	138.5	121.9	19	34
L1-C	17.6	131.0	139.4	120.9	18	30
L1-D	17.1	131.1	139.3	121.6	21	33
L2-F	17.2	130.0	138.0	118.8	18	29
L2-G	17.1	129.5	137.4	118.3	18	37
L2-H	17.8	129.8	137.5	118.0	17	34
Equatorial axis, (Transverse)						
T1-A	17.7	129.9	137.7	120.3	19	34
T1-B	17.6	130.6	138.4	121.9	17	30
T1-C	17.6	131.7	139.4	120.4	19	32
^a T1-D	17.8	-135.2	-135.6	Loaded in compression to 1 percent, strain control.		
T1-E	17.9	129.5	^b 132.4	Loaded in tension to 2 percent, strain control.		
T2-G	17.5	129.5	^b 135.7	Strain controlled simulation of SN011		
Average	17.5	130.3	138.5	120.2	18	32
Std Dev	0.3	0.7	0.8	1.5	1.5	2.3
CV, %	1.6	0.6	0.6	1.2	8.1	7.2

^aNot included in average values.

^bMaximum value observed during simulation, not included in the average.

TABLE 3.—TENSILE PROPERTIES OF THE MEMBRANE REGION, 1 INCH GAGE SECTION

SN029 2152	Young's modulus, E Msi	0.2% Yield strength, S_{ys} Ksi	Ultimate strength, S_u ksi	Fracture stress, S_f ksi	Elongation, e_f %	Area reduction, RA %
Polar axis, (Longitudinal)						
L3-1	16.2	129.4	146.9	126.8	----	29
L3-8	16.8	130.9	146.6	129.3	16.2	27
L3-10	17.5	133.0	150.8	131.5	16.1	29
L4-3	16.5	130.4	148.9	129.2	----	32
L4-2	16.1	131.4	149.7	128.7	14.1	32
L4-9	17.0	130.8	147.0	128.0	15.2	32
L3-5 ^b	18.5	131.5	145.5	127.0	16.7	27
L4-5 ^b	17.7	134.1	146.0	126.7	14.5	26
Equatorial axis, (Transverse)						
T3-8	17.3	132.2	147.6	130.1	16.2	29
T3-2	17.8	133.3	151.2	132.6	15.5	28
T3-6	17.2	132.5	148.9	129.7	16.8	30
T4-10	17.3	129.2	146.5	128.7	----	32
T4-3	16.6	131.5	149.4	128.1	16.2	32
T4-1	17.8	128.3	144.3	123.2	18.1	33
Average	17.1 ^a	131.3	147.8	128.5	16	30
Std Dev	0.7	1.5	1.9	1.8	0.9	2.1
CV, %	4.3	1.1	1.3	1.4	5.9	7.1

^aLarge initial curvature of the test specimens likely lowered the measured Young's modulus. Elongation is the average of measurements from both sides of the specimen.

^bAnnealed at 635 °C for 2 hr in argon.

TABLE 4.—YOUNG'S MODULUS, YIELD STRENGTH, ULTIMATE STRENGTH, FRACTURE STRENGTH, ELONGATION, AREA REDUCTION AND FRACTURE TOUGHNESS OF 1970 VINTAGE ALPHA-BETA AND BETA Ti-6Al-4V PLATE FORGED TO 3.5 INCH THICKNESS

[See appendix for additional data.]

Alpha-beta forged and mill annealed					
E , Msi	17.21±0.21				
S_{ys} , S_u , S_f ksi	131.1±3.3; 140.0±0.7; 130.1±4.8				
e_f , RA , %	12.2±2.0; 23.9±1.7				
B , in (thickness)	0.5	1.0	1.5	2.0	3.0
^a K_{Ic} , ksi√in	67.6±2.7	70.8±6.1	91.6	86.3±2.6	83.4, 84.0
Beta forged and mill annealed					
E , Msi	17.23±0.14				
S_{ys} , S_u , S_f ksi	129.7±1.0; 137.4±0.4; 133.6±1.3				
e_f , RA , %	10.2±1.0; 14.0±1.3				
B , in (thickness)	0.5	1.0	1.5	2.0	3.0
^a K_{Ic} , ksi√in	62.6±6.7	72.2±2.8	95.6±2.8	93.2±3.1	96.8, 101

^aThe 0.5 in. values did not meet E399 requirements associated with plastic zone size and stable crack extension (i.e. 2.5 (K_Q/S_{ys}) and P_{max}/P_Q) and thus are conditional or K_Q values.

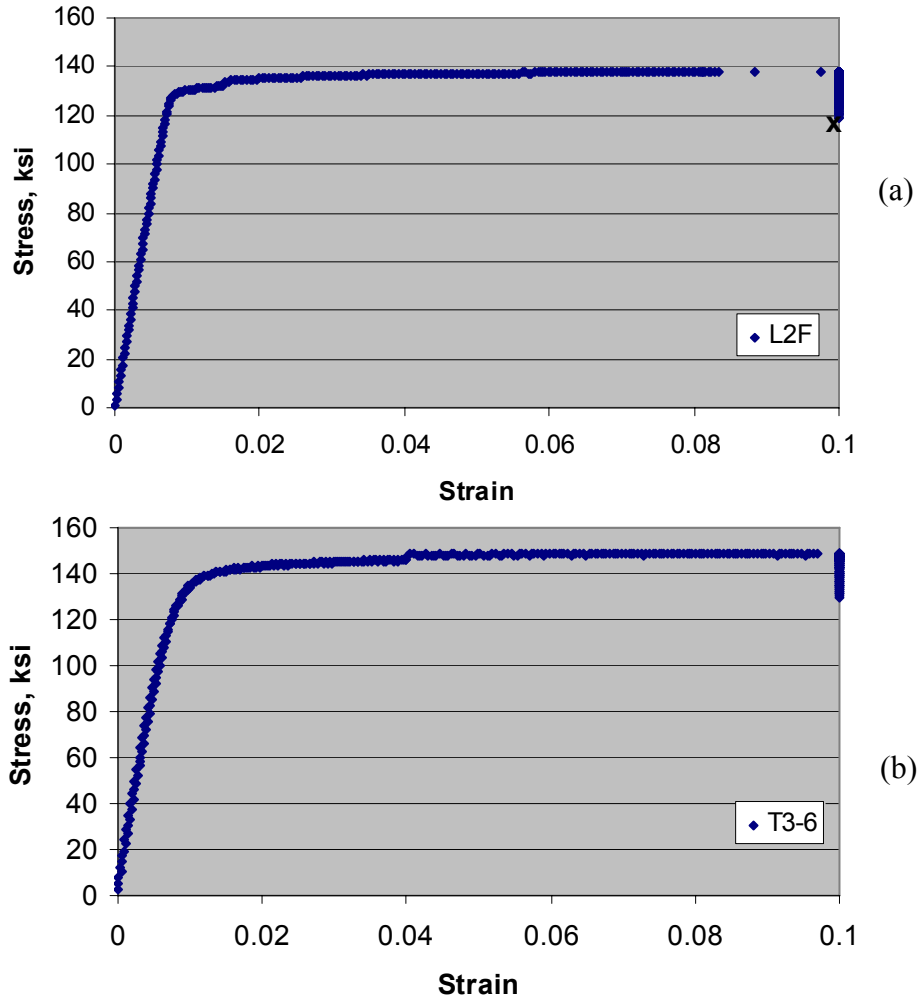


Figure 14.—Typical tensile stress-strain curve for the (a) boss-transition region and (b) membrane region with strain recorded to 10 percent.

The effect of range of data used in regression, which is generally less than 2 percent, can be seen in table 5. A consistent difference in modulus between polar (L) and equatorial (T) orientations can also be seen in the data, however, the difference is not significant above an 89 percent level, and thus not significantly different for engineering purposes (significance at 95 percent confidence).

To confirm the extensometer results, one specimen was strain gaged on both sides and loaded in the elastic range (± 85 ksi). The estimated Young's modulus and Poisson's ratio were 17.7 Msi and 0.27 respectively in tension, and 17.8 Msi and 0.28 respectively in compression, in good agreement with the extensometer results. Dynamic Young's modulus and Poisson's ratio as determined via resonance of two wide beams from the boss region were 17.3 Msi and 0.26 at room temperature, again in reasonable agreement. Measurements on six narrow beams gave Young's modulus of 17.1 ± 0.2 Msi. The effect of temperature on the dynamic Young's modulus, shear modulus and Poisson's ratio are shown in figure 15. Young's modulus and shear modulus as functions of temperature can be described by

$$E(\text{Msi}) = 17.425 - 0.0042 T \quad (75 \text{ to } 1650 \text{ } ^\circ\text{F}) \quad (5)$$

$$G(\text{Msi}) = 6.886 - 0.0016 T \quad (75 \text{ to } 1650 \text{ } ^\circ\text{F}) \quad (6)$$

TABLE 5.—EFFECT OF STRESS RANGE ON CALCULATED YOUNG’S MODULUS FOR THE BOSS-TRANSITION REGION

SN029	Young’s modulus, E , Msi				
	Data range used in regression, ksi				
	10 to 65	10 to 115	40 to 115	70 to 115	80 to 120
L1A	17.4	17.2	17.1	17.1	17.0
L1B	17.7	17.4	17.2	17.1	16.9
L1C	17.9	17.6	17.4	17.2	17.1
L1D	17.2	17.1	17.0	17.0	16.9
L2F	17.3	17.2	17.0	16.9	16.8
L2G	17.2	17.1	17.0	16.9	16.6
L2H	17.9	17.8	17.6	17.4	17.2
T1A	18.1	17.7	17.4	17.3	17.0
T1B	17.8	17.6	17.4	17.3	17.1
T1C	17.9	17.6	17.4	17.2	17.1
T1D ^a (compression)	17.8	17.8	17.8	17.7	17.6
T1E	18.1	17.9	17.7	17.5	17.4
T2G	17.7	17.5	17.5	17.4	17.3
Average =	17.7	17.5	17.3	17.2	17.0
Std Dev =	0.3	0.3	0.3	0.2	0.2
CV, % =	1.8	1.6	1.5	1.2	1.2

^aNot included in average value.

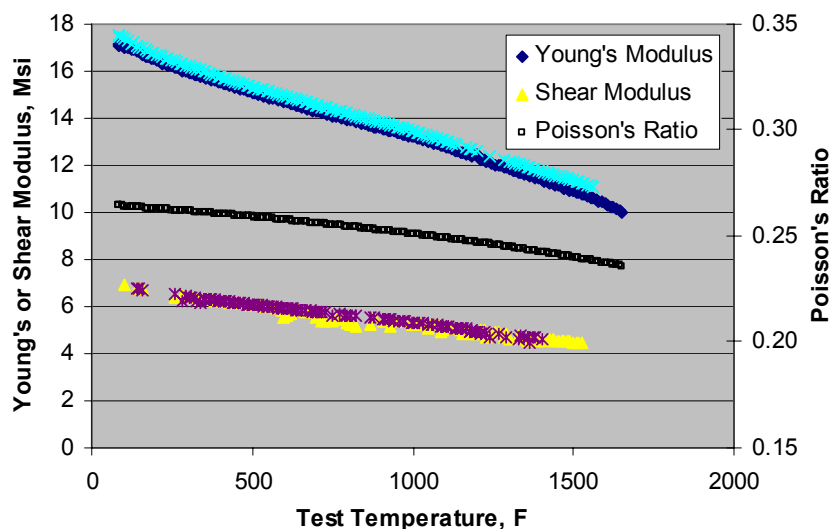


Figure 15.—Young’s modulus, shear modulus and calculated Poisson’s ratio as a function of temperature for the boss-transition region.

where T is the temperature in °F. Possible explanations for the elevated Young’s modulus are texture developed during forging of the tank hemispheres and effects of autofrettage. In order to check for texture, which was not strongly evident in metallographic sections, the basal plane pole figures in figures 16 and 17 were constructed. Although the pole figures indicate different basal plane distributions in the membrane and boss-transition regions, relatively weak multiples-of-random-distribution of ~ 1.85 were measured (versus 1.0 for random material), implying that the measured properties, which are comparable to those of relatively thick forged plate, are representative of Ti-6Al-4V without heavy texture.

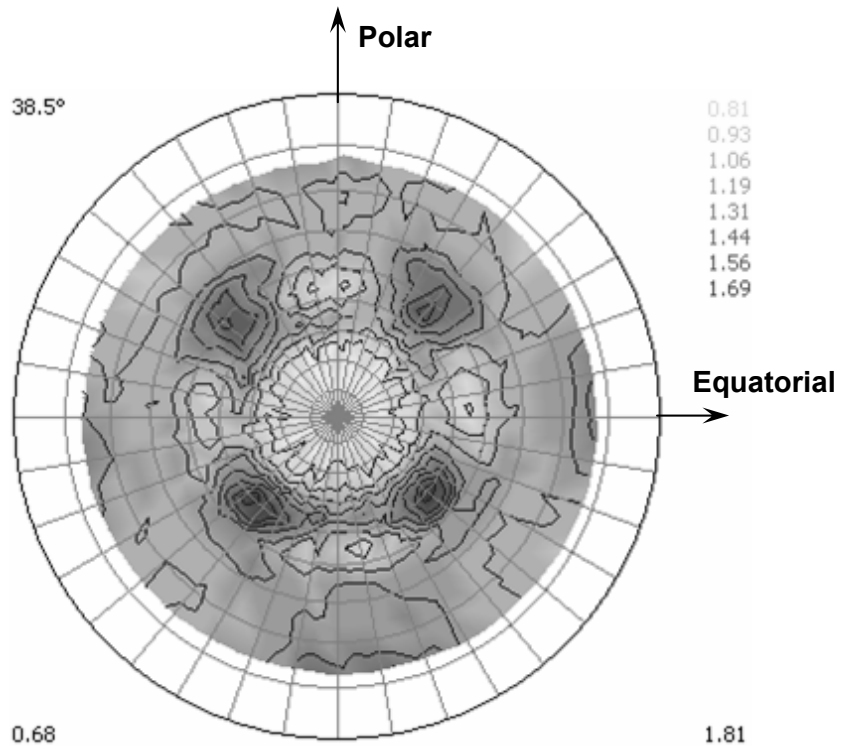


Figure 16.—Alpha phase pole figure of the boss transition region.

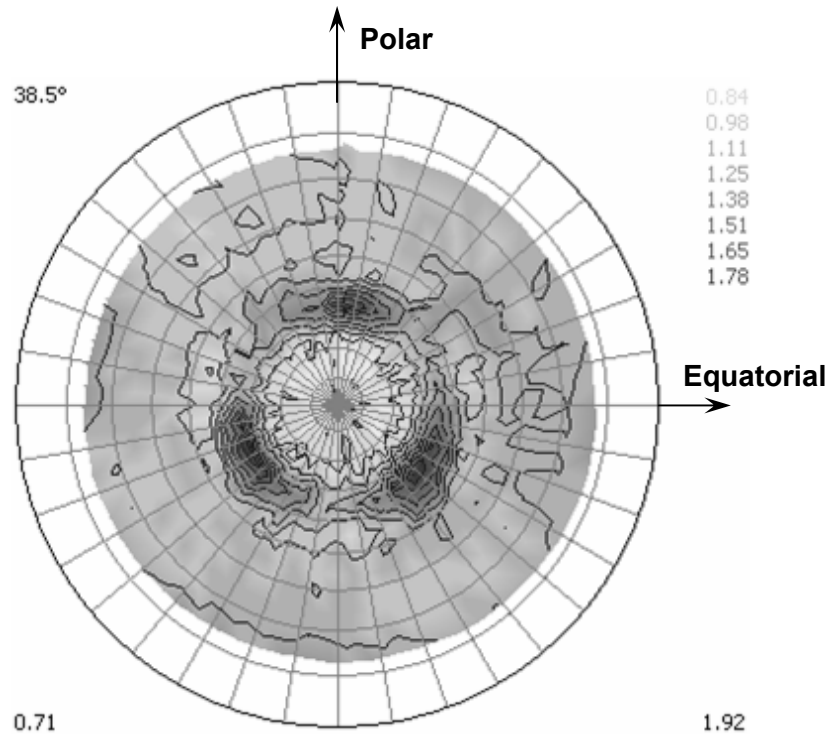


Figure 17.—Alpha phase pole figure of the membrane region.

Cyclic Loading

Bauschinger effect and proof cycle simulation

The Bauschinger effect is the reduction of yield strength after loading past yield in the opposite direction. It can be particularly significant for aluminum and titanium alloys. An example of the effect for the Ti-6Al-4V liner is shown in figure 18 where, after yielding in compression, tensile yield occurs more gradually and at substantially lower stresses (~85 ksi) than the usual 130 ksi. This results in a change in load sharing between the Kevlar overwrap and liner with multiple yield cycles, as occurred during the testing of SN011 (ref. 6).

Simulation of burst testing of vessel SN011

To experimentally simulate the burst testing of COPV SN011 at WSTF and thereby explain some of the observations (ref. 6), equations (1) to (4) were applied for a vessel, biaxial proof strain of 1.2 percent, which is typically used in autofrettage. This gives an equivalent uniaxial strain of 2 percent. The post-autofrettage compressive strain was based on MEOP and the observed biaxial strain range of 0.7 percent during burst testing of SN011. This gives an equivalent uniaxial strain of 1 percent.

The uniaxial simulation is shown in figure 19. The test implies that the liner does exhibit reduced yield when reloaded to near proof pressure, and thus explains the observation of low vessel yield during burst testing. The Ti-6Al-4V liner material specimen, however, did sustain the desired loads and strains without catastrophic failure.

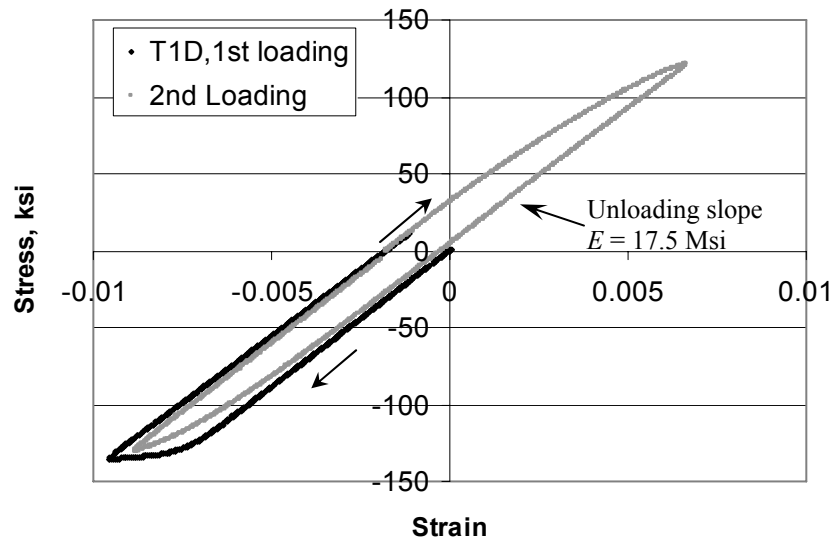


Figure 18.—Load cycle exhibiting the Bauschinger effect. The first cycle was compression. The second cycle was tension followed by compression.

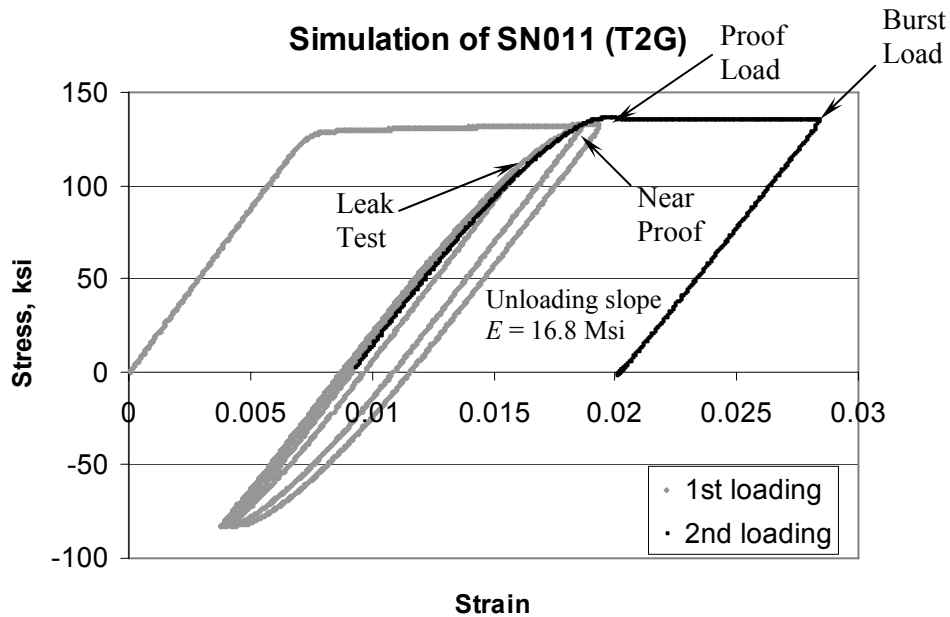


Figure 19.—Uniaxial, strain controlled simulation of SN011 burst test.

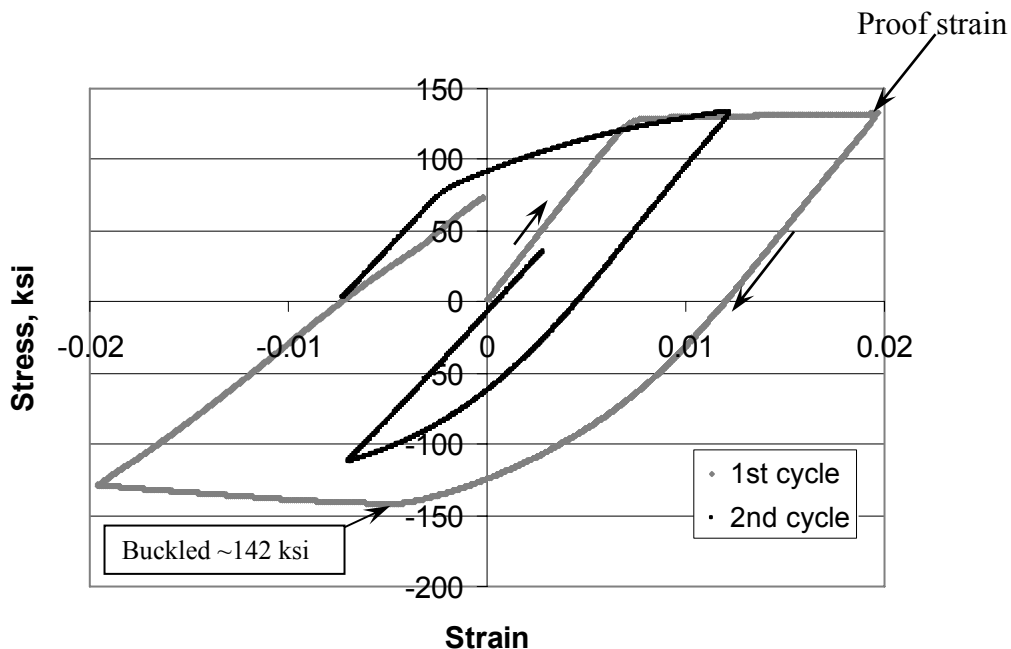


Figure 20.—Load history of the buckled test specimen.

Post-buckling fatigue loading

The proof and buckling cycles are shown in figure 20, and the severely buckled specimen is shown in figure 21. The specimen exhibited a maximum unconstrained bending displacement of 0.024 in., whereas upon clamping in fixed grips the displacement was reduced to 0.008 in., which is somewhat larger than that observed on the surface of SN029 (fig. 3).

The post-buckling, cyclic load-controlled history is shown in figure 22. A uniaxial strain range of 1 percent was sought based on the biaxial operating range of 0.7 percent and equations (1) to (4). Initial

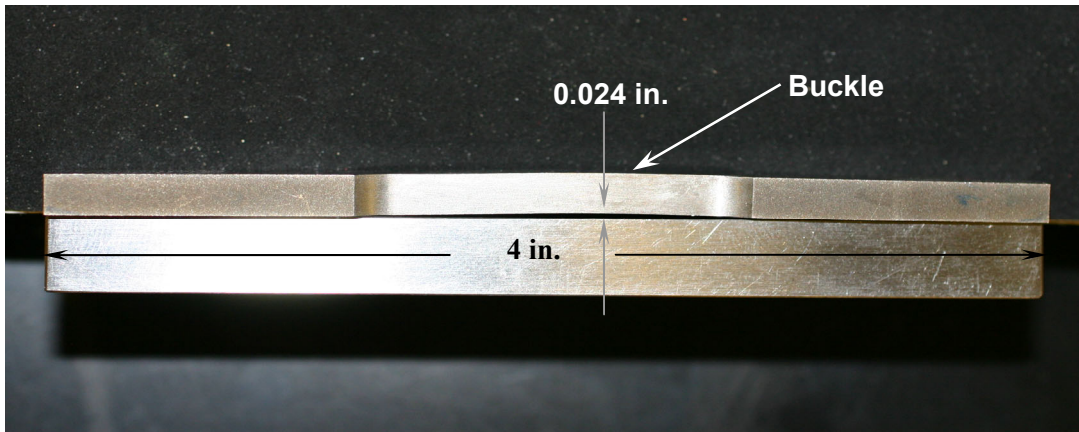


Figure 21.—Buckled test specimen.

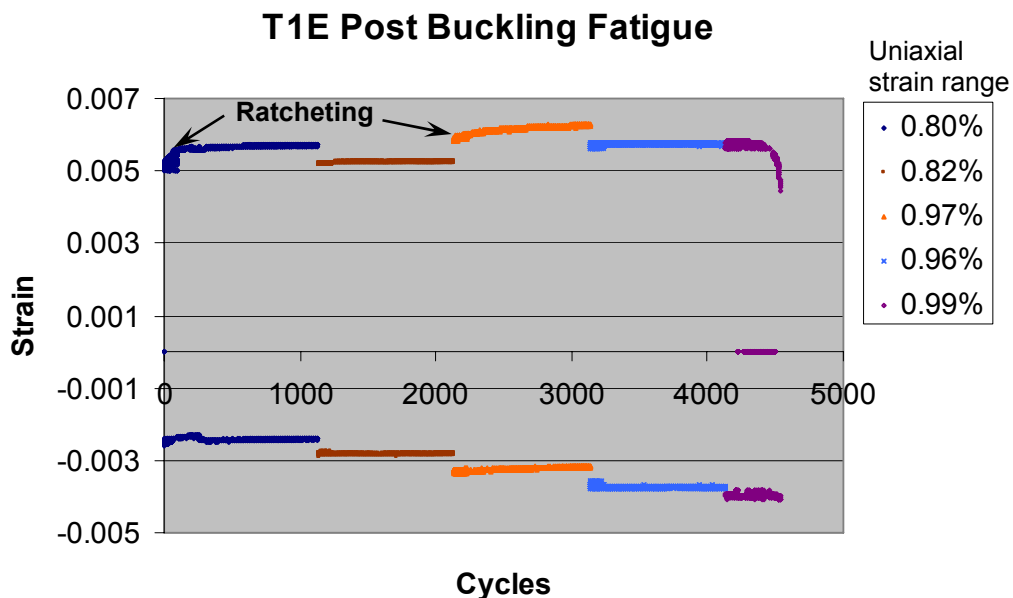


Figure 22.—Cyclic load history of the buckled test specimen under load control.

calculations based on figure 19 did not provide sufficient strain range due to work hardening of the material. Thus subsequent blocks of 1000 cycles were applied with increasing load levels until 1 percent was attained.

Some strain ratcheting was apparent after each increase in the load range, and a loss of strain range can be seen before failure. This is the result of a fatigue crack becoming large enough to cause a non-uniform strain across the section. The buckled tensile specimen survived ~2,100 cycles at >0.8 percent uniaxial strain range followed by ~2,400 cycles at >0.96 percent uniaxial strain range. The stress levels corresponding to the strain ranges in each block were -56 to 99 ksi for 0.80 percent, -57 to 99 ksi for 0.82 percent, -69 to 110 ksi for 0.97 percent, -77 to 105 ksi for 0.96 percent, and -81 to 105 ksi for 0.99 percent.

Final failure occurred from a corner crack (crack dimensions of $a = 0.09$ in. and $c = 0.11$ in.) at the start of the transition radius, well away from the buckle after 4,536 cycles, as shown in figure 23. The expected strain range as a function of applied cycles for a smooth specimen subjected to rotational bending at 170 °F can be estimated from (ref. 7):

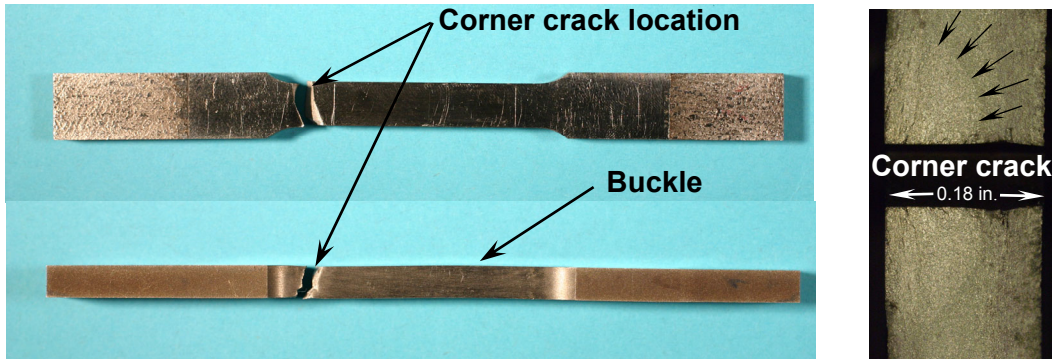


Figure 23.—Fractured test specimen and fatigue crack.

$$\frac{\Delta\varepsilon}{2} = 2.8519(2N_f)^{-0.90337} + 0.01987(1 - 8.042 \times 10^{-6} \sigma_o)(2N_f)^{-0.12293} \quad (5)$$

where $\Delta\varepsilon$ is the applied strain range, N_f is the applied cycles, and σ_o is the applied mean stress. If the function is assumed to be applicable to the COPV liner, then a 1 percent strain range is expected to have a 13,000 cycle life, implying that either specimen configuration (tensile versus bending) and preparation, and/or the buckle has reduced the measured fatigue life.

In addition to the post buckling fatigue test, several remnant tensile specimens were cyclically loaded to failure in strain control between 0.0058 and -0.0041 . Unfortunately, due to a less than optimal design for studying low cycle fatigue, all the specimens failed from the transition radius despite attempts to smooth the radius and slightly reduce the gage section. Nevertheless, the samples had longer failure lives than required for this COPV application: for five membrane specimens, the average cycles-to-failure was $3,592 \pm 721$, with a range of 3,045 to 4,744 cycles. Testing of one boss region specimen resulted in 12,494 cycles to failure.

Fracture Toughness Estimation

Failure of the buckled specimen from a fatigue crack provides an opportunity to estimate fracture toughness. The failure load (105 ksi) and the crack size were used with the design codes AFGROW (ref. 8) and NASGRO (ref. 9) to calculate the results in table 6. The codes give a stress intensity of 60 to 86 $\text{ksi}\sqrt{\text{in}}$ under conditions of net section yield, and the NASGRO results vary surprisingly with the configuration solution chosen. Despite the net section yield and thin section used (0.182 by 0.248 in.), the estimates are in reasonable agreement with plane strain fracture toughness data generated via ASTM E399-81 (71 to 92 $\text{ksi}\sqrt{\text{in}}$ shown in table 4 for alpha-beta forged and mill annealed material) and maximum stress intensities measured with thin sheets (ref. 10). However, the estimates are somewhat higher than the 50 $\text{ksi}\sqrt{\text{in}}$ value reported for the instability asymptote of fatigue crack growth curves generated with 1 in. thick compact tension specimens (ref. 11).

It is noteworthy that the measured fracture toughness of Ti-6Al-4V is a strong function of the operational procedure and crack extension used, and it is difficult to measure K_{Ic} per ASTM E399 with a thickness less than 1 in. This is a result of the large ductility and R-curve exhibited by Ti-6Al-4V, in combination with the use of 2 percent crack extension, rather than a plane stress to plane strain transition effect. The use of a crack extension based on the specimen size results in thick specimens exhibiting higher, rather than lower, values of measured fracture toughness because the longer extension drives the result up the R-curve.

TABLE 6.—ESTIMATES OF FRACTURE TOUGHNESS DETERMINED WITH AFGROW AND NASGRO. $K_I(a)$ AND $K_I(c)$ ARE THE STRESS INTENSITIES AT THE a AND c CRACK TIPS. $\phi(a)$ AND $\phi(c)$ ARE THE CORRESPONDING PARAMETRIC ANGLES USED IN THE CALCULATIONS

Code and crack configuration	$K_I(a)$ Ksi√in	$K_I(c)$ ksi√in	$\phi(a)$	$\phi(c)$
AFGROW 1070	74	71	83	5
“ “ “ 3020	74	73		
NASGRO CC01	57	54	90	0
“ “ “ CC05	86	80		
“ “ “ CC09	60	56	87	3

This can be observed in results from 0.5 in. thick specimens made from the material used to generate the data in table 4: The 0.5 in. specimens indicated conditional fracture toughness values² of $K_Q = 67.6 \pm 2.7$ ksi√in for alpha-beta forging and 62.6 ± 6.7 ksi√in for beta forging, somewhat lower than measurements from thicker specimens (table 4).

Munz (ref. 10) et al. measured K_Q values and crack growth resistance curves for forged and annealed Ti-6Al-4V plate and found that K_Q associated with thickness ranging from 0.080 to 1.65 in. fell within the band of the R-curve, and that small changes in the extension (0.008 in.) resulted in large changes in the stress intensity (20 ksi√in), clearly implying that crack extension rather than thickness dominates measured values over a wide thickness range. If an absolute extension is used, then more consistent values might be attained, regardless of sheet thickness. However, further study is needed to determine the best method for characterizing fracture toughness of Ti-6Al-4V for use with analyses such as NASGRO.

Conclusions

To improve modeling efforts of the shuttle COPV's, a detailed characterization of the Ti-4V-6Al liner material was conducted. Chemical, microstructural, static and cyclic properties were investigated. The chemistry of the liner is normal and there was no evidence of alpha case or measurable surface embrittlement. The mechanical properties are consistent with those of other annealed Ti-6Al-4V.

Tensile specimens subjected to cyclic loading failed from corner cracks, but at lives greater than those expected in service. Cyclic loading of a buckled, boss-transition region tensile specimen at loads similar to those expected in COPV service indicated more than adequate lifetime. Fatigue failure occurred from a corner crack that developed in the transition radius rather than in the buckled region.

The observed, surface oxidation and the microcracks on the tank interior did not degrade the measured tensile properties: excellent elongation was exhibited. The microcracks do not appear to be the result of measurably increased oxygen or carbon very near the interior surface. Their cause is currently unknown, however, the oxide layer and autofrettage cycle are suspected.

For engineering purposes, Young's modulus and Poisson's ratio of the Ti-6Al-4V in SN029 are 17.5 Msi and 0.28, for both tensile and compressive loading. The measured Young's modulus is somewhat higher than values in published literature, but agrees with 1980's measurements made at GRC on 1970 vintage Ti-6Al-4V forged plate. The increased values were not due to a strong texture. The yield strength, ultimate strength and nominal fracture toughness in the boss-transition region were 130 ksi, 135 ksi and 74 ksi√in, in good agreement with literature and tests performed at GRC on 1970 vintage Ti-6Al-4V forged plate.

² K_Q values are those that don't meet ASTM E399 requirements. In this case, the requirements not meet were associated with plastic zone size and stable crack extension (i.e. $2.5 (K_Q/S_{ys})$ and P_{max}/P_Q).

Appendix

True stress-strain tensile properties for the mill annealed Ti-6Al-4V materials described in table 4 are given in table A1, and the microstructures are shown in figures A1 and A2. The following equations were used for true stress at maximum load, σ_u , true fracture stress, σ_f , true uniform strain at maximum load, ϵ_{ut} , true uniform plastic strain at maximum load, ϵ_{up} , and the true fracture strain, ϵ_f :

$$\sigma_u = \frac{P_{\max}}{A_u} \quad (\text{A1})$$

$$\sigma_f = \frac{P_f}{A_m} \quad (\text{A2})$$

$$\epsilon_{ut} = \ln \frac{A_o}{A_u} \quad (\text{A3})$$

$$\epsilon_{up} = \ln(1 + e_{lp}) \quad (\text{A4})$$

$$\epsilon_f = \ln \frac{A_o}{A_m} \quad (\text{A5})$$

where A_o is the initial cross sectional area, A_m is the minimum area after fracture, e_{lp} is the longitudinal plastic strain at maximum load, L_u is the length a maximum load and A_u is the uniform area:

$$A_U = \frac{L_o}{L_u} A_o \quad (\text{A6})$$

TABLE A1.—TRUE STRESS-STRAIN TENSILE PROPERTIES OF 1970 VINTAGE ALPHA-BETA AND BETA
TI-6AL-4V PLATE FORGED TO 3.5 INCH THICKNESS.
[The gage length and diameter were 2 and 0.5 inch, respectively]

Young' modulus, Msi	% Offset yield strength, ksi				True stress at max load, σ_u , ksi	True fracture stress, σ_f , ksi	True uniform total strain at max load, ϵ_{ut}	True uniform plastic strain at max load, ϵ_{up}	True Fracture Strain, ϵ_f
	0.05	0.1	0.2	0.5					
Alpha-beta forged and mill annealed									
17.2±0.2	125.3±4.2	128.4±3.7	131.1±3.3	134.0±2.6	148.3±2.2	170.8±4.0	.057±.016	.049±.015	.273±.022
Beta forged and mill annealed									
17.3±0.1	121.4±1.0	125.8±1.1	129.5±1.2	133.5±0.7	145.9±1.6	155.3±0.9	.058±.009	.050±.010	.151±.015

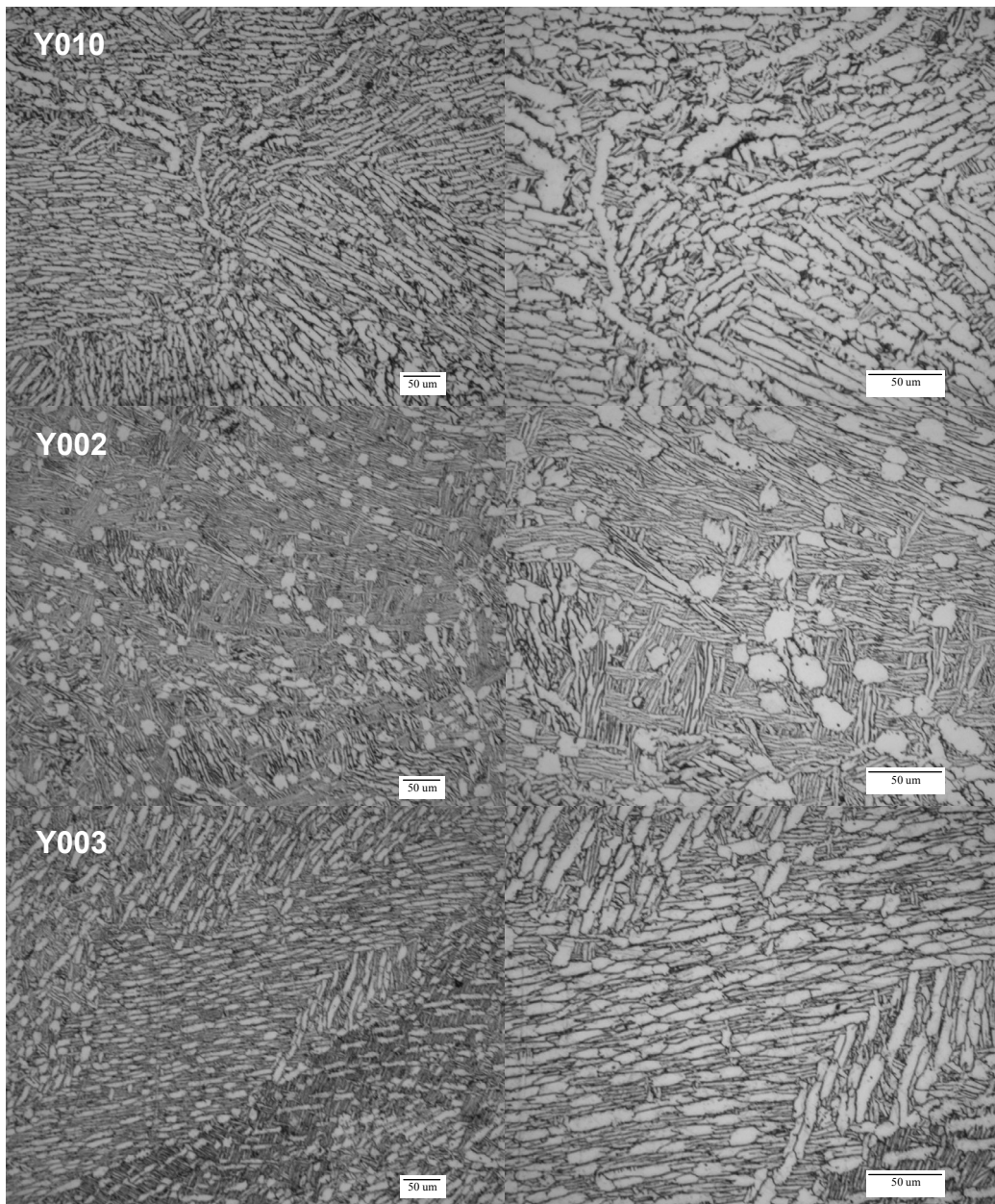


Figure A1.—Microstructure of 1970 vintage alpha-beta Ti-6Al-4V plate forged to 3.5 in. thickness.

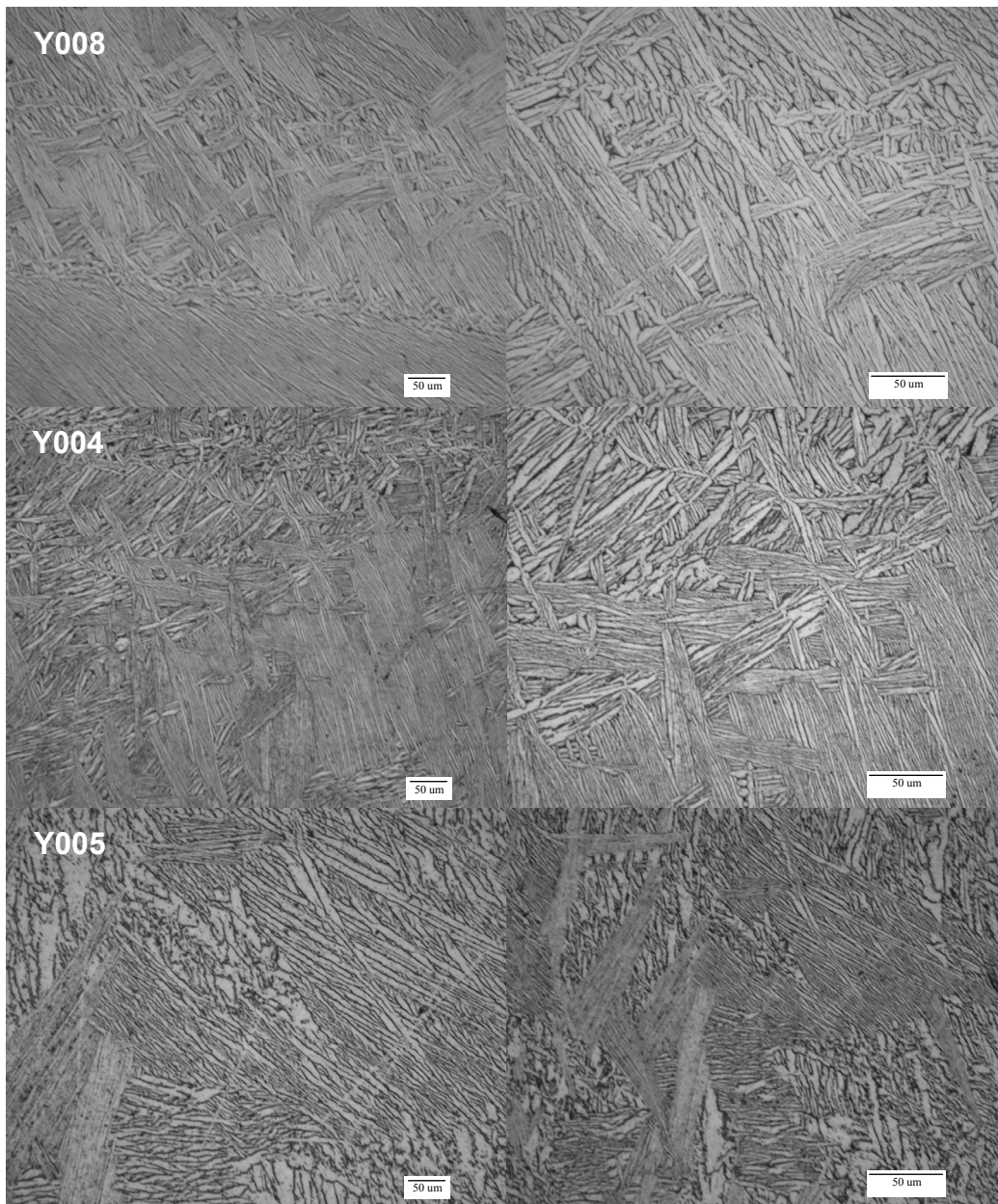


Figure A2.—Microstructure of 1970 vintage beta Ti-6Al-4V plate forged to 3.5 in. thickness.

References

1. ASTM E8, in Annual Book of Standards, volume 03.01, American Society for Testing and Materials, W. Conshohocken, Pennsylvania (2003).
2. ASTM E1876, in Annual Book of Standards, volume 03.01, American Society for Testing and Materials, W. Conshohocken, Pennsylvania (2003).
3. H.W. Rosenberg, "Properties and Processing of Ti-6Al-4V," TIMET Corp, Pittsburgh, PA, 1978.
4. J.A. Salem, unpublished work on strength and fracture toughness of titanium—6 percent aluminum—4 percent vanadium in heat treated and mill annealed conditions, 1983.
5. D.N. Williams and R.A. Wood, "Effects of Surface Condition on the Mechanical Properties of Titanium and its Alloys," Metals and Ceramics Information Center, MCIC-71-01, August 1971.
6. Mark R. Leifeste, WSTF Post-Burst Analysis of 40 in. OMS He COPV s/n 011, 2007.
7. J. Walcher, D. Gray, S. Manson, "Aspects of Cumulative Fatigue Damage Analysis of Cold End Rotating Structures," Paper 79-1190 in Proceedings of AIAA/SAE/ASME 15th Joint Propulsion Meeting, Las Vegas, NV, June 18–20, 1979.
8. AFGROW Fracture Mechanics and Fatigue Crack Growth Analysis software, version 4.0011.14, Wright-Patterson Air Force Base, Ohio.
9. NASGRO Fracture Mechanics and Fatigue Crack Growth Analysis Software, version 5.1, Southwest Research Institute, San Antonio, Texas.
10. D. Munz, K.H. Galda, and F. Link, "Effect of Specimen Size on Fracture Toughness of a Titanium Alloy," in Mechanics of Crack Growth, ASTM STP 590, 1976, pp. 219–234.
11. R.E. Lewis, J.G. Bjeletich, T.M. Morton, and F.A. Crossley, "Effect of Cooling Rate on Fracture Behavior of Mill-Annealed Ti-6Al-4V, in Cracks and Fracture, ASTM STP 601, 1976, pp. 371–390.

REPORT DOCUMENTATION PAGE			Form Approved OMB No. 0704-0188		
The public reporting burden for this collection of information is estimated to average 1 hour per response, including the time for reviewing instructions, searching existing data sources, gathering and maintaining the data needed, and completing and reviewing the collection of information. Send comments regarding this burden estimate or any other aspect of this collection of information, including suggestions for reducing this burden, to Department of Defense, Washington Headquarters Services, Directorate for Information Operations and Reports (0704-0188), 1215 Jefferson Davis Highway, Suite 1204, Arlington, VA 22202-4302. Respondents should be aware that notwithstanding any other provision of law, no person shall be subject to any penalty for failing to comply with a collection of information if it does not display a currently valid OMB control number. PLEASE DO NOT RETURN YOUR FORM TO THE ABOVE ADDRESS.					
1. REPORT DATE (DD-MM-YYYY) 01-03-2008		2. REPORT TYPE Technical Memorandum		3. DATES COVERED (From - To)	
4. TITLE AND SUBTITLE Strength, Fatigue, and Fracture Toughness of Ti-6Al-4V Liner From a Composite Over-Wrapped Pressure Vessel			5a. CONTRACT NUMBER		
			5b. GRANT NUMBER		
			5c. PROGRAM ELEMENT NUMBER		
6. AUTHOR(S) Salem, Jonathan, A.; Lerch, Brad; Thesken, John, C.; Sutter, Jim; Russell, Richard			5d. PROJECT NUMBER		
			5e. TASK NUMBER		
			5f. WORK UNIT NUMBER WBS 981155.01.03.04		
7. PERFORMING ORGANIZATION NAME(S) AND ADDRESS(ES) National Aeronautics and Space Administration John H. Glenn Research Center at Lewis Field Cleveland, Ohio 44135-3191			8. PERFORMING ORGANIZATION REPORT NUMBER E-16307		
9. SPONSORING/MONITORING AGENCY NAME(S) AND ADDRESS(ES) National Aeronautics and Space Administration Washington, DC 20546-0001			10. SPONSORING/MONITORS ACRONYM(S) NASA		
			11. SPONSORING/MONITORING REPORT NUMBER NASA/TM-2008-215147		
12. DISTRIBUTION/AVAILABILITY STATEMENT Unclassified-Unlimited Subject Category: 26 Available electronically at http://gltrs.grc.nasa.gov This publication is available from the NASA Center for AeroSpace Information, 301-621-0390					
13. SUPPLEMENTARY NOTES					
14. ABSTRACT It was demonstrated by way of experiment that Composite Over-wrapped Pressure Vessel (COPV) Ti-6Al-4V liner material can sustain the expected service loads and cycles. The experiments were performed as part of investigations on the residual life of COPV tanks being used in Space Shuttle Orbiters. Measured properties included tensile strength, compressive strength, reversed loading cycles to simulate liner proof strains, and cyclic fatigue loading to demonstrate the ability to sustain 1000 cycles after liner buckling. The liner material came from a salvaged 40 in. Columbia (orbiter 102) tank (SN029), and tensile strength measurements were made on both boss-transition (thick) and membrane regions (thin). The average measured yield strength was 131 ksi in the boss-transition and membrane regions, in good agreement with measurements made on 1970's vintage forged plate stock. However, Young's modulus was 17.4±0.3 Msi, somewhat higher than typical handbook values (~16 Msi). The fracture toughness, as estimated from a failed fatigue specimen, was 74 ksi√in, in reasonable agreement with standardized measurements made on 1970's vintage forged plate stock. Low cycle fatigue of a buckled test specimen implied that as-imprinted liners can sustain over 4000 load cycles.					
15. SUBJECT TERMS Metal fatigue; Tensile strength; Fracture toughness; Modulus of elasticity; Poisson's ratio; Titanium-6 percent Aluminum-4 percent Vanadium; Composite over-wrap pressure vessels; Microstructure; Space shuttle					
16. SECURITY CLASSIFICATION OF:			17. LIMITATION OF ABSTRACT	18. NUMBER OF PAGES	19a. NAME OF RESPONSIBLE PERSON
a. REPORT	b. ABSTRACT	c. THIS PAGE			STI Help Desk (email:help@sti.nasa.gov)
U	U	U	UU	32	19b. TELEPHONE NUMBER (include area code) 301-621-0390

